CHAPTER 137

FLOW SEPARATION, WAKE VORTICES AND PRESSURE DISTRIBUTION AROUND A CIRCULAR CYLINDER UNDER OSCILLATORY WAVES

Yuichi Iwagaki Professor

and

Hajime Ishida Research Assistant

Department of Civil Engineering Kyoto University Kyoto, Japan

ABSTRACT

Flow separation of a laminar boundary layer on the surface of a circular cylinder developed by monochromatic waves has been investigated both theoretically and experimentally, and next, characteristics of vortex formation and shedding have been discussed with Keulegan-Carpenter's number and Reynolds number, and finally, local depressions of the wave pressure around the cylinder induced by wake vortices have been examined in the experiment.

INTROOUCTION

A number of studies have been made with respect to wave forces on marine structures, especially on a circular cylinder. However, in order to estimate the wave forces more correctly, it is necessary to make clear the mechanism of wave force action. For this purpose, it is important, as the first step, to investigate the transformation of waves by the circular cylinder and induced flow along the cylinder, and next, to evaluate the magnitude of pressures acting on the cylinder exerted by such an affected wave field.

In case of steady flow, it has already been ascertained that both the behavior of fluid around a cylinder and forces on it are principally subject to Reynolds number $Re = U\partial/v$, in which U:flow velocity, ∂ :diameter of cylinder and v:dynamic viscosity. Son and Hanratty¹,²) indicated that in the range of lower Reynolds number the position of separation point moves forward from the back stagnation point with increase in Reynolds number. For instance when Re = 500, the angle of separation point from the front stagnation point 80° .

Then it is well known that such a separation causes wake vortices and their configurations are also subject to Reynolds number; that is, a pair of symmetric and stable vortices is formed at values of Re lower than 40 and Karman vortex street appears at values of Rebetween about 70 and 2500^{3} . In this case, the frequency of vortex generation is known by using Strouhal number determined by Reynolds number⁴).

Hereupon, corresponding to such patterns of fluid motion, the distributions of pressure and shearing stress around a cylinder are determined. Among the fluid forces on the cylinder, the drag force due to the shearing stress is predominant in the range of lower Reynolds number. However, with increase in Reynolds number, another kind of drag force becomes predominant owing to depression of pressure induced by wake vortices at the rear part of the cylinder. It is too familiar to state that these results are shown by a figure in text books as the relationship between the drag coefficient and Reynolds number⁴).

COASTAL ENGINEERING-1976

On the other hand, in case of wave fields, the separation point, the behavior of wake vortices and the pressure distribution have not been made so clear that there exist unkown facts about the correspondence of the drag and inertia coefficients to the conditions of fluid motion.

From this point of view, in the present study, general characteristics of the flow separation of a laminar boundary layer on the surface of a circular cylinder developed by monochromatic waves are shown by using the theory presented by the authors in the previous paper⁵), and then, experimental results of the separation point obtained by taking photographs using the method of flow visualization are compared with the theoretical ones, and next, vortex formation and shedding are investigated by means of successive photography. Finally, wave pressure distributions around the cylinder are measured by using a small pressure gauge and depressions of the pressure induced by wake vortices are discussed.

FLOW SEPARATION

1. THEORY

The coordinate system is shown in <u>Fig.1</u>. Denoting the water particle velocity in the boundary layer along the cylinder in the polar coordinate (θ, π, z) or in the boundary layer coordinate (x, y, z) by u, the separation point of a streamline in the boundary layer is generally determined by the condition that



The authors have already obtained the second approximate solution of the water particle velocity in the boundary layer in the following dimensionless form by means of the boundary layer approximations and the perturbation method in the previous paper⁵):

 $u_{2nd} = u_0 + \varepsilon_1 u_1 ,$



Fig.1 Coordinate system.

2342

OSCILLATORY WAVES

$$\zeta_{1d}^{\prime} = -\frac{7i}{4}e^{-\sqrt{2}(1+i)n'} + \frac{3i}{2}e^{-(1+i)n'} + \frac{1-i}{2}n'e^{-(1+i)n'} + \frac{i}{4}e^{-2(1+i)n'},$$

$$\zeta_{1b}^{\prime} = -\frac{3}{4}\frac{1}{4}e^{-2n'} + e^{-n'}(\frac{1}{2}\cos n' + 2\sin n') - \frac{n}{2}e^{-n'}(\cos n' - \sin n'),$$

$$\zeta_{1c}^{\prime} = -\frac{3}{4}\frac{1}{4}e^{-2n'} + e^{-n'}(\cos n' - \frac{1}{2}\sin n') + \frac{n}{2}e^{-n'}(\cos n' + \sin n'),$$

$$\zeta_{1e}^{\prime} = -\frac{1}{2}+e^{-n'}(\frac{1}{2}\cos n' + \sin n') - \frac{n}{2}e^{-n'}(\cos n' - \sin n'),$$

$$\eta^{\prime} = ky\sqrt{Re^{*}/2},$$
(7)

in which, ε_1 :very small quantity of the order of the wave steepness in magnitude, ε_2 :very small quantity of the order of the ratio of the boundary layer thickness to the radius of cylinder in magnitude, σ_1 angular frequency, H:wave height, L:wave length, T:wave period, R:radius of cylinder, k:wave number, Re^{*}(= c/vk):convenient Reynolds number using the wave celerity c instead of the fluid velocity, and U_0 and W_0 :amplitudes of dimensionless velocities derived by eliminating both the dimensional part $\pi H/T$ and time variation part $e^{L\sigma T}$ from the water particle velocities of diffracted waves on the surface of cylinder in the direction of the coordinates X and z respectively. Suffixes x and z indicate differentiations with respect to X and z respectively, and \wedge and \vee indicate real and imaginary parts respectively.

By applying this velocity u_{2nd} to the velocity u in Eq.(1), Eq.(1) is rewritten as follows:

$$\partial u_{2nd}/\partial \eta \left|_{\eta'=0} = \partial u_0/\partial \eta \left|_{\eta'=0} + \varepsilon_1 \partial u_1/\partial \eta'\right|_{\eta'=0} = 0.$$
 (8)

Using Eq.(3) and Eq.(4), $\partial u_0 / \partial \eta'|_{\eta'=0}$ and $\partial u_1 / \partial \eta'|_{\eta'=0}$ are expressed as follows:

$$\begin{aligned} & \left| u_{0}/\partial n^{\prime} \right|_{n^{\prime}=0} = \left\{ 1+i\right\} u_{0} e^{i\sigma t} , \\ & \left| u_{1}/\partial n^{\prime} \right|_{n^{\prime}=0} = \left\{ \varepsilon_{2}/\varepsilon_{1} \right\} \frac{1}{\sqrt{2}} u_{0} e^{i\sigma t} \\ & + \left\{ 1-\frac{1}{\sqrt{2}} \right\} \left\{ 1-i\right\} \left\{ u_{0}u_{0_{x}} + \omega_{0}u_{0_{z}} \right\} e^{2i\sigma t} + \left\{ \frac{5}{2} - \frac{7\sqrt{2}}{4} \right\} \left\{ 1-i\right\} \left\{ u_{0}u_{0_{z}} - \omega_{0}u_{0_{z}} \right\} e^{2i\sigma t} \\ & + \frac{1}{2} \left\{ \left(\hat{u}_{0}\hat{u}_{0_{x}} + \hat{u}_{0}\hat{u}_{0_{x}} \right) + \left(\hat{w}_{0}\hat{u}_{0_{z}} + \hat{w}_{0}\hat{u}_{0_{z}} \right) \right\} - \frac{1}{2} \left\{ \left(\hat{u}_{0}\hat{u}_{0_{x}} - \tilde{u}_{0}\hat{u}_{0_{z}} \right) \right\} \left\{ \cdots \right\} \left\{ 1-i\right\} \left\{ u_{0}\hat{u}_{0_{x}} - \tilde{u}_{0}\hat{u}_{0_{x}} \right\} \right\} . \\ & \left\{ 1-\frac{1}{\sqrt{2}} \left\{ \left(\hat{u}_{0}\hat{u}_{0_{x}} + \hat{u}_{0}\hat{u}_{0_{x}} \right) + \left(\hat{w}_{0}\hat{u}_{0_{z}} + \tilde{w}_{0}\hat{u}_{0_{z}} \right) \right\} \right\} - \frac{1}{2} \left\{ \left(\hat{u}_{0}\hat{u}_{0_{x}} - \tilde{u}_{0}\hat{u}_{0_{x}} \right) + \left(\hat{u}_{0}\hat{w}_{0_{z}} - \tilde{u}_{0}\hat{w}_{0_{z}} \right) \right\} \right\} . \\ & \left\{ 1-\frac{1}{\sqrt{2}} \left\{ \left(\hat{u}_{0}\hat{u}_{0_{x}} + \tilde{u}_{0}\hat{u}_{0_{x}} \right) + \left(\hat{u}_{0}\hat{u}_{0_{z}} + \tilde{u}_{0}\hat{u}_{0_{z}} \right) \right\} \right\} - \frac{1}{2} \left\{ \left(\hat{u}_{0}\hat{u}_{0_{x}} - \tilde{u}_{0}\hat{u}_{0_{x}} \right) + \left(\hat{u}_{0}\hat{u}_{0_{z}} - \tilde{u}_{0}\hat{u}_{0_{z}} \right) \right\} \right\} \\ & \left\{ 1-\frac{1}{\sqrt{2}} \left\{ \left(\hat{u}_{0}\hat{u}_{0_{x}} + \tilde{u}_{0}\hat{u}_{0_{x}} \right) + \left(\hat{u}_{0}\hat{u}_{0_{z}} - \tilde{u}_{0}\hat{u}_{0_{z}} \right) \right\} \right\} \right\} \\ & \left\{ 1-\frac{1}{\sqrt{2}} \left\{ \left(\hat{u}_{0}\hat{u}_{0_{x}} + \tilde{u}_{0}\hat{u}_{0_{x}} \right) + \left(\hat{u}_{0}\hat{u}_{0_{x}} - \tilde{u}_{0}\hat{u}_{0_{x}} \right) \right\} \right\} \\ & \left\{ 1-\frac{1}{\sqrt{2}} \left\{ \left(\hat{u}_{0}\hat{u}_{0_{x}} + \tilde{u}_{0}\hat{u}_{0_{x}} \right) \right\} \right\} \\ & \left\{ 1-\frac{1}{\sqrt{2}} \left\{ 1-\frac{1}{\sqrt{2}} \left(\hat{u}_{0}\hat{u}_{0_{x}} + \tilde{u}_{0}\hat{u}_{0_{x}} \right) \right\} \right\} \\ & \left\{ 1-\frac{1}{\sqrt{2}} \left\{ 1-\frac{1}{\sqrt{2}} \left(1-\frac{1}{\sqrt{2}} \left(1-\frac{1}{\sqrt{2}} \right) \right\} \right\} \\ & \left\{ 1-\frac{1}{\sqrt{2}} \left(1-\frac{1}{\sqrt{2}} \left(1-\frac{1}{\sqrt{2}} \left(1-\frac{1}{\sqrt{2}} \left(1-\frac{1}{\sqrt{2}} \right) \right) \right\} \right\} \\ & \left\{ 1-\frac{1}{\sqrt{2}} \left(1-\frac{1}{\sqrt{2}} \left(1-\frac{1}{\sqrt{2}} \left(1-\frac{1}{\sqrt{2}} \right) \right) \right\} \\ & \left\{ 1-\frac{1}{\sqrt{2}} \left(1-\frac{1}{\sqrt{2}} \left(1-\frac{1}{\sqrt{2}} \left(1-\frac{1}{\sqrt{2}} \left(1-\frac{1}{\sqrt{2}} \right) \right) \right\} \\ & \left\{ 1-\frac{1}{\sqrt{2}} \left(1-\frac{1}{\sqrt{2}} \left(1-\frac{1}{\sqrt{2}} \left(1-\frac{1}{\sqrt{2}} \left(1-\frac{1}{\sqrt{2}} \right) \right) \right\} \\ & \left\{ 1-\frac{1}{\sqrt{2}} \left(1-\frac{1}{\sqrt{2}} \left(1-\frac{1}{\sqrt{2}} \left(1-\frac{1}{\sqrt{2}} \left(1-\frac{1}{\sqrt{2}} \left(1-\frac{1}{\sqrt{2}$$

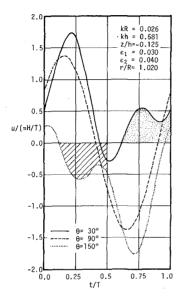
It is impossible to express the separation point θ_8 explicitly from Eq.(8) so that the separation point is obtained as the point that the sign of left hand side of Eq.(8) is just changed in varying θ by 1° in computations.

2. COMPUTATIONS AND DISCUSSIONS

<u>Fig.2</u> shows an example of the time variation of the water particle velocity in the boundary layer u_{2nd} . In this case, Keulegan-Carpenter's number $([K.C.]_m = U_{max}T/P)$ is 6. The water particle velocity at $\theta = 150^{\circ}$ denoted by a dotted line becomes negative value after t/T is about 0.125, which means the occurrence of flow separation behind the cylinder and the generation of subsequent reverse current. On the other hand, the water particle velocity at $\theta = 30^{\circ}$ denoted by a solid line becomes positive during the phase of wave trough, which also means the occurrence of flow separation. The shadow regions in this figure show the duration and intensity of these reverse currents.

<u>Fig.3</u> shows an example of the time variation of flow separation point with a parameter of Keulegan-Carpenter's number (hereafter, it is denoted as K.C. number for abbreviation). As the water particle velocity varies in magnitude with the wave phase, the separation

point proceeds from behind of the cylinder to front of the cylinder with increase in t/T during the phase of wave crest and its reverse movement is seen during the phase of wave trough. Especially when K.C. number is small, for example 3, the separation point varies quickly in the wide range, and this phenomenon is peculiar to flow separation under oscillatory waves. The reason may be explained by the fact that the phase of the water particle velocity in the boundary layer proceeds faster than the phase of ambient velocity. On the other hand, when K.C. number is large, for example 15, the separation point does not vary so widely, which is similar to the flow separation in steady flow.



<u>Fig.2</u> Variation of water particle velocity u_{2nd} in boundary layer with time.

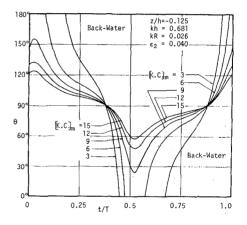


Fig.3 Variation of flow separation point with time.

Fig.4 shows the shift of separation point due to K.C. number, in which the phase t/T is fixed to 0.25 and kR is taken as a parameter. In this figure, for example, when kR is 0.01, the flow separation does not occur if K.C. number is smaller than 2, and with increase in K.C. number, the separation point moves from 180° toward 90°. And finally it approaches to a definite point asymptotically for each kR. If K.C. number is constant, it is found that the smaller kR, the smaller angle of separation point; that is, the wake region behind the cylinder becomes wider. In this calculation, it is also found that Reynolds number $U_{max}D/v$ and the relative water depth kh do not much affect the separation point.

<u>Fig.5</u> shows the vertical distributions of separation point. If we consider the case that $\frac{h}{h} = 40$ cm, $\mathcal{D} = 3$ cm and v = 0.01112 cm²/sec, the wave period of each curve becomes 0.5 sec v 5.0 sec as shown in the figure. In this calculation, K.C. number at the position where z/h = -0.1 is 6. In the figure, when the wave period is as short as 0.5 sec or 0.7 sec, the flow separation occurs only near the water surface. On the other hand, when the wave period is as long as 2 sec or 5 sec, the separation point does not change vertically so much. This is caused by the vertical distributions of water particle velocity of the main flow, which means vertical change of K.C. number.

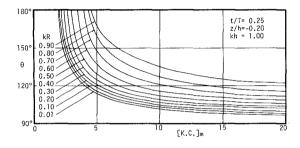


Fig.4 Shift of flow separation point.

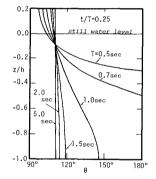


Fig.5 Vertical distributions of flow separation point.

3. EXPERIMENTS AND CONSIDERATION

In the experiment of flow separation, a circular cylinder made of Lucite with a diametr of 3 cm was installed in the center of a wave tank, which is 27 m long, 50 cm wide and 70 cm deep. As shown in <u>Fig.6</u>, from this cylinder surface, a platinum wire with a diameter 6 0.05 mm was stretched horizontally, and trains of hydrogen bubbles were generated from the platinum wire by using a pulse generator, and photographs were taken through the glass bottom. As the cylinder was made rotatable around the vertical z-axis in <u>Fig.1</u>, the separation point was examined by rotating the cylinder every 5° in the range of angle from 90° to 160° during the phase of wave crest.

The water depth h was 40 cm and the measuring point z_p was 5 cm below still water level, and the correspondence of experimental cases to the wave characteristics is shown in <u>Table 1</u>, in which $Re_m = U_{max} D/v$.

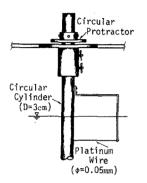


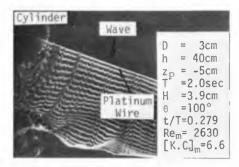
Fig.6 Sketch of experimental apparatus for flow separation.

Table 1 Experimental condition for flow separation.

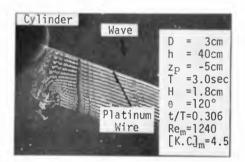
	h=40 cm,		$z_p = -5 \text{ cm}$	
Case	T(sec)	H(cm)	[K.C.]m	Rem ×10-3
I- 1	2.0	1.5~1.6	2.5~ 2.7	I.02~1.09
I— 2	2.0	2.4~2.6	4.1~ 4.4	1.64~1.77
I- 3	2.0	3.3~3.4	5.6~ 5.7	2.25~2.32
I 4	2.0	3.7~3.9	6.2~ 6.6	2.49~2.63
I 5	2.0	4.9~5.1	8.3~ 8.6	3.30~3.44
I- 6	2.0	5.7~5.8	9.6~ 9.8	3.84~3.91
I— 7	3.0	1.0~I.I	2.5~ 2.8	0.69~0.76
I— 8	3.0	1.8~2.0	4.5~ 5.0	1.24~1.38
I— 9	3.0	2.5~2.7	6.2~ 6.7	1.73~1.87
I—10	3.0	3.5~3.8	8.7~ 9.5	2.42~2.63
I11	3.0	4.5~4.9	11.2~12.2	3.11~3.39

Some examples of photographs taken about flow separation are shown in <u>Photo.1(a)</u>, (b) and (c). <u>Photo.1</u>(a) shows that when t/T = 0.279, the flow is not separated yet at the position of the platinum wire where $\theta = 100^\circ$, in which K.C. number is 6.6. <u>Photo.1(b)</u> is an example of such a critical condition that the flow is just separated at the position of platinum wire, in which t/T = 0.306, $\theta = 120^\circ$ and K.C. number is 4.5. <u>Photo.1(c)</u> is the case when t/T = 0.323 and the position of the platinum wire, $\theta = 125^\circ$, is in the region of reverse current because of flow separation, in which K.C. number is 4.8.

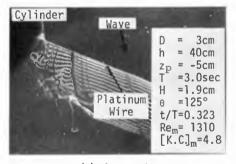
OSCILLATORY WAVES



(a) Not separated.



(b) Critical.



(c) Separated.

Photo.1 Visualization of flow separation.

COASTAL ENGINEERING-1976

Fig.7 shows the comparison between theoretical separation points and experimental values. In this figure, experimental data are divided into three flow conditions by the photographs; that is, at the intersection point of the platnum wire and the cylinder surface, the separation has not occured yet, just occured and already occured as shown in <u>Photo.1</u>(a), (b) and (c) respectively. This figure indicates that the experimental values agree well with the theoretical ones except Cases I-6, I-10 and I-11, in which K.C. numbers are so large that the vortices generated before a half period of waves in front of the cylinder become to disturb the boundary layer during their shedding along the cylinder surface toward the rear part of the cylinder by the return flow.

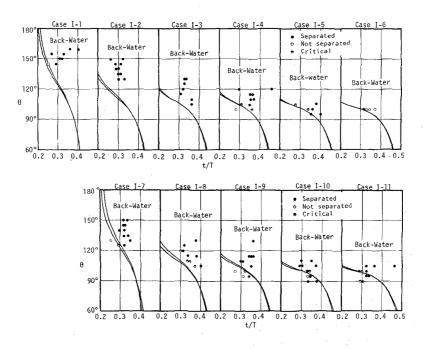


Fig.7 Comparison of theoretical flow separation point with experimental data.

WAKE VORTICES

1. EXPERIMENT

In the experiment of wake vortices, platinum wires were stretched horizontally from the cylinder surface at the angles of about 90° and 270°, and photographs of hydrogen bubble lines were taken successively with an interval of about 0.25 sec by using a moter driven camera. Other experimental apparatus were same as in the case of flow separation. Experimental conditions were as follows: h = 40 cm, $z_p = -5$ cm, v = 0.01141 cm²/sec, and the wave period T in the range from 1 sec to 8 sec and the wave hight H from 1.5 cm to 7.5 cm were used in this experiment.

Examples of successive photographs showing the time process of vortex formation and shedding are shown in <u>Photo.2</u> and <u>Photo.3</u>, which are an example of a pair of symmetric vortices and that of extremely asymmetric vortices or almost Karman vortex street respectively.

From <u>Photo.2</u>, it is recognized that after flow separation, a new pair of vortices begins to form behind the cylinder at the phase t/T = 0.30 and is growing up symmetrically till t/T = 0.50, in which another pair of vortices at the right side of each photographs is an old one generated in front of the cylinder before a half period of waves and transported by main flow, and that as the main flow changes its direction after t/T = 0.5, the vortices are transported toward the front of the cylinder at each side of the cylinder. In this case, K.C. number is 7.4.

On the other hand, it is recognized from <u>Photo.3</u> that a pair of small vortices appears slightly at the phase t/T = 0.15, but only one vortex at the lower side of the cylinder in the photographs is growing large till t/T = 0.23 and begins to shed at t/T = 0.31, and the other vortex at the upper side of the cylinder in the photographs is growing till t/T = 0.51. In this case, K.C. number is as large as 19.8, and hydrogen bubble lines are quite turbulent because of the remaining effects of some vortices generated before a half period of waves.

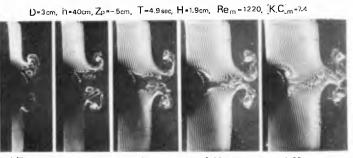
2. DISCUSSION OF RESULTS

The relationship between vortex configurations and both Reynolds number \Re_m and K.C. number $[K.C.]_m$ is shown in <u>Fig.8</u>(a). The explanation of each symbol is shown in <u>Fig.8</u>(b), in which dotted lines show the path of vortices in return flow. In this figure, it is found that the vortex configurations are generally transformed by K.C. number; that is, when K.C. number is smaller than 2, flow separation does not occur both theoretically and experimentally, and when K.C. number is smaller than about 7.5, a pair of symmetric vortices appears. With increase in K.C. number, a pair of vortices becomes asymmetric, especially when K.C. number is larger than 15, it becomes extreamly asymmetric as shown in Vortex-Pattern C, and finally, when K.C. number reaches about 20, vortices become similar to Karman vortex street.

It is apparent that such transformations of vortex configuration are caused by the characteristics of vortex generation and shedding. The former is closely related to the characteristics of flow separation and the latter is due to the sweeping effect of a main flow and the stability of vortices. In other wards, when K.C. number is small, the flow separation does not continue so long time as to form vortices, and even when Reynolds number is high to some extent, the wake vortices may not be formed so easily in the wave field as in the steady flow. On the other hand, as the angle of separation point becomes smaller with increase in K.C. number and does not vary so quickly with the wave phase which means that the wake region becomes larger for a longer time, the generation and shedding of wake vortices in the wave field become similar to those in steady flow.

It is considered that the state of vortex shedding in the wave field may be known by using the relationship between Reynolds number and Strouhal number obtained in the case of steady $flow^{6)}$. Denoting the frequency of vortex shedding, the wave frequency and Strouhal

COASTAL ENGINEERING-1976

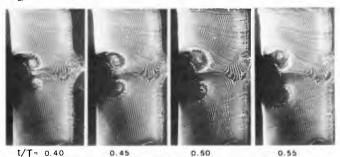


t/T= 0.15 0.20 _

0,25

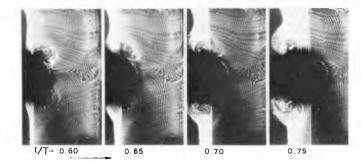
0.30

0.35

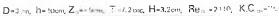


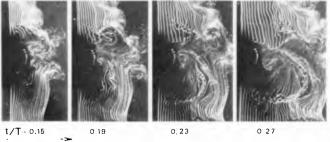
t/T = 0.40

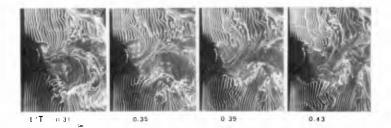
0.55

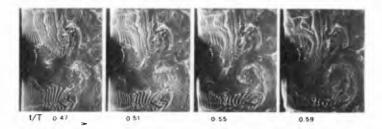


 $\frac{Photo.2}{a \text{ pair of symmetric vortices.}} \ \ Time \ \ variation \ \ of \ \ wake \ vortices.$









 $\frac{Photo.3}{Karman} \ \ \, \mbox{Time variation of wake vortices in case of Karman vortex street.}$

number by $f_{\rm S},$ f and S respectively, the value of $f_{\rm S}/f$ means the number of shedding vortex during one wave period, which is estimated by the following equation:

$$f_s/f = (Re/Re_m) \cdot S \cdot [K.C.]_m$$
,(11)

in which the validity of Eq.(11) is easily confirmed by substituting Re = UD/ν , Rem = UmD/ν , S = f_SD/U and [K.C.]_m = $U_m/(Df)$ into the right hand side of Eq.(11).

Therefore, $f_s/f = 2$ corresponds to the condition that a pair of vortices are generated during a half period of wave and the direction of flow in the wave field is reversed just before a subsequent vortex appears, which is considered to be similar to the configuration of Vortex-Pattern C. The dotted line denoted by $f_s/f = 2$ in Fig.8(a) shows the condition in the case of applying the average value of Re during a half period and the value of S corresponding to Rem, which corresponds well to Vortex-Pattern C appearing when [K.C.]m is about 16.

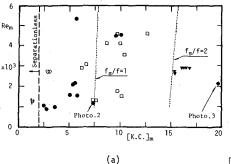
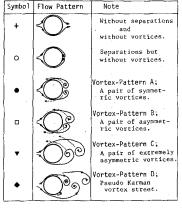


Fig.8 Variation of vortex-pattern behind cylinder with K.C. number and Reynolds number.



(b)

PRESSURE DISTRIBUTION

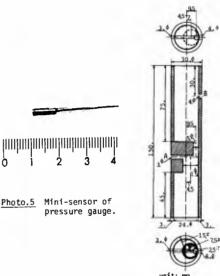
1. EXPERIMENT

In the experiment of wave pressure measurements, a wave tank which is 17.5 m long, 1.5 m wide and 75 cm deep was used, in which, a circular cylinder consisting of three parts, as shown in <u>Photo.4</u>, with a diameter of 3 cm and a total length of 85 cm was installed vertically at the position of 9 m and 25 cm apart from the wave generator paddle and the side wall respectively. A very small pressure gauge with a diameter of 2.8 mm ahown in <u>Photo.5</u> was attached to the surface of the middle cylinder part at the position A shown in <u>Fig.9</u>, and its linearity was confirmed to be very well.

Distributions of wave pressure were measured by rotating this cylinder intermittently around the center axis, and then, the water depth h was 40 cm and the measuring point z_p was 5 cm below still water level. In Table 2, wave height H, wave period T, K.C. number, Reynolds number and the angle of separation point calculated theoretically at the wave phase t/T = 0.25 are shown correspondingly to each experimental case.



Photo.4 Experimental apparatus for wave pressure.



A; Probe B; Cord

Fig.9 Cross section of middle part of cylinder.

a - - 5 am

Table 2 Experimental condition for wave pressure.

h = 40 cm

		<i>n</i> -40 cm	1,	$z_p 5$ cm	L.
Case	T(sec)	H(cm)	[K.C] _m	Rem [×] 10−3	θ_{s} (t/T=0.25)
III 1	0.7	3.5	2.6	2.77	147°
III— 2	0.7	7.5	5.3	5.80	115°
111 3	1.0	3.8	3.5	2.71	128
III 4	1.0	8.7	8.0	6.25	106°
111 5	1.5	3.3	4.2	2.21	120"
111-6	1.5	6.5	8.6	4.43	105°
III- 7	2.0	3.0	5.1	2.01	115°
III- 8	2.0	7.9	13.3	5.30	100°
111 9	2.5	3.0	6.1	1.96	110°
III-10	2.5	6.0	12.5	3.90	100°

2. DISCUSSION OF RESULTS

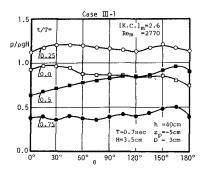
In the analysis of experimental data, it is assumed that the wave conditions are constant even if the angle of measuring point is changed, and the value of wave pressure at each angle is determined by averaging the data during three cycles of successive waves.

Some examples of pressure distributions around the cylinder at the wave phases t/T = 0, 0.25, 0.5 and 0.75 are shown in Fig.10(a) and (b), and correspondingly, time variations of wave pressure at the angles $\theta = 30^{\circ}$, 90° and 150° are shown in Fig.11(a) and (b). In each figure, (a) and (b) show the results of Cases III-1 and III-7 respectively.

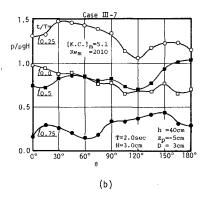
In Case III-1, Reynolds number is 2770 and K.C. number is as small as 2.6. In this case, flow separation occurs but any wake vortex does not appear distinctly, and therefore, pressure distributions are roughly smooth as shown in <u>Fig.10(a)</u> and time variations of pressure are almost sinusoidal as shown in <u>Fig.11(a)</u>, corresponding to the water level variation.

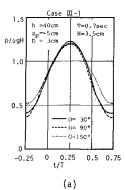
In Case III-7, Reynolds number is 2010 and K.C. number is 5.1. In this case, a pair of symmetric vortices appears and causes local depressions of wave pressure; that is, in $\underline{Fig.10}(b)$, the pressures at the angles $\theta = 120^{\circ}$ and 60° are extreamly decreased by each wake vortex at the wave phases t/T = 0.25 and 0.75 respectively. And moreover, it is found in $\underline{Fig.11}(b)$ that the time variation curve of wave pressure at $\theta = 150^{\circ}$ fluctuates near t/T = 0.25, which is also regarded as the effect of wake vortices.

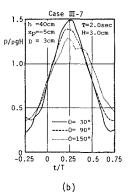
It is understood from these examples that wake vortices cause the local depressions of wave pressure and induce the drag force, and moreover, it is considered that if wake vortices neither vanish nor shed soon and remain near $\theta = 0^\circ$ or 180° even when t/T = 0 or 0.5 respectively, the inertia force tends to decrease due to their vortices. This phenomenon may occur in the case of Vortex-Pattern C.

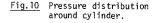












.

Fig.ll Pressure variation with time.

CONCLUSION

As a process of making clear the generation mechanism of wave forces acting on a circular cylinder, following the previous study of the water particle velocity in the laminar boundary layer, the characteristics of flow separation, wake vortices and wave pressure have been investigated, and the results obtained are as follows:

1. The separation point of the laminar boundary layer developed by wave motion on the cylinder is mainly varied with the wave phase and K.C. number. When K.C. number is small, apparent flow separation occurs so that the separation point varies quickly in short time. However, when K.C. number becomes large, the variation of separation point with the wave phase becomes more gradual and characteristics of flow separation become similar to those in steady flow.

2. Experimental values of separation point agree well with the theoretical ones in the case when K.C. number is smaller than about 9. However, when K.C. number becomes larger, the difference between both values becomes noticeable by the reason that wake vortices generated before a half period of waves disturb the boundary layer during their reverse shedding.

3. Within the range of this experiment, the configuration of wake vortices is successively transformed from a pair of symmetric vortices to asymmetric ones and finally Karman vortex street with increase in K.C. number. Generally speaking, the configuration of wake vortices is subject to the ratio of the frequency of vortex generation to the wave frequency, which may be determined by K.C. number, Reynolds number and Strouhal number.

4. Wave pressures around a cylinder are affected by wake vortices and the dynamic pressure in addition to the static pressure caused by water level variation. Wake vortices induce local pressure depressions in the wave field as well as in steady flow, and therefore, it is considered that fully developed vortices may cause to not only increase the drag force but also decrease the inertia force.

ACKNOWLEOGEMENT

The authors wish to express their gratitudes to Mr. W. Kioka and Mr. Y. Motoyama for their assistances through the experiments. This work was partly supported by Scientific Research Funds from the Ministry of Education.

REFERENCES

- 1) Son, Jaime S., and Thomas J.Hanratty: Velocity gradients at the wall for flow around a cylinder at Reynolds numbers from 5×10^3 to 10^5 , Jour. Fluid Mech., Vol.35, Part 2, pp.353-368, 1969.
- Son, Jaime S., and Thomas J.Hanratty: Numerical solution for the flow around a cylinder at Reynolds numbers of 40, 200 and 500, Jour. Fluid Mech., Vol.35, Part 2, pp.369-386, 1969.
- 3) Batchelor,G.K.: An Introduction to Fluid Dynamics, Cambridge University Press, pp.343-353, 1967.
- 4) Schlichting, H.: Boundary Layer Theory, McGrow-Hill, 1968.
- Iwagaki,Y., and H.Ishida: Laminar boundary layer around a circular cylinder under oscillatory waves, Proc. 14th Coastal Eng. Confer. ASCE, Vol.3, pp.1848-1862, 1974.
- 6) Keulegan, G.H., and L.H.Carpenter: Forces on cylinders and plates in an oscillating fluid, Jour. Res. Nat. Bur. Stand., Vol.60, No.5, pp.423-440, May 1958.